Received: 22 September 2017 | Revised: 4 May 2018 | Accepted: 30 June 2018

DOI: 10.1002/jnm.2479

RESEARCH ARTICLE

WILEY

New formulations for the hybrid meshless-MoM method applied to 2D scattering problems

Ursula do Carmo Resende[1] | Fernando José da Silva Moreira[2] | Márcio Matias Afonso[1] | Eduardo Henrique da Rocha Coppoli[1]

[1]Department of Electrical Engineering, Federal Center for Technological Education of Minas Gerais, Belo Horizonte, MG 35510-000, Brazil

[2]Department of Electronics Engineering, Federal University of Minas Gerais, Belo Horizonte, MG 31270-901, Brazil

Correspondence
Ursula do Carmo Resende, Department of Electrical Engineering, Federal Center for Technological Education of Minas Gerais, Belo Horizonte, MG 35510-000, Brazil.
Email: resendeursula@cefetmg.br

Funding information
CAPES, Grant/Award Number: 068419/2014-01; FAPEMIG; CNPq

Abstract

In this work, new formulations for the hybrid meshless-method of moments technique are presented. The proposed approaches are applied for solving 2D electromagnetic scattering problems. The solution is obtained by dividing the problem into 2 subproblems: one internal to the scatterer and another external to it. For the internal subproblem, the meshless method is used for solving the weak form of the 2D Helmholtz equation. For the external subproblem, the Method of Moments is used for solving different combinations of electric field integral equation and magnetic field integral equation. Both subproblems are coupled by imposing the continuity of the tangential fields over the scatterer surface. The technique is applied for solving the TMz electromagnetic scattering by an infinite dielectric cylinder. Numerical and analytical results are compared to each other showing the validity and accuracy of the proposed approaches.

KEYWORDS

CFIE, EFGM, electromagnetic scattering, hybrid methods and meshless methods

1 | INTRODUCTION

The problem of electromagnetic scattering by conducting, inhomogeneous, lossy, and arbitrarily shaped dielectric bodies has been extensively dealt with in the past. For scatterers that are neither small nor large compared to the wavelength, a rigorous solution of Maxwell's equations is required. Using integral equation methods, such as the method of moments (MoM), this kind of unbounded problem can be evaluated very successfully. Meanwhile, if the scatterer has complex inhomogeneities, these methods become computationally intensive.[1] On the other hand, complex structures and inhomogeneities are well treated by differential equation methods, such as the finite element method (FEM) and finite difference time domain (FDTD). However, those methods alone are more suitable for bounded problems, as they cannot incorporate the Sommerfeld radiation condition. Then, it is necessary to extend the discretization domain by creating a fictitious boundary at some distance away from the scatterer, where this condition is approximately imposed.[2]

Considering the advantages and disadvantages of integral and differential techniques, the use of hybrid techniques is a suitable way to simulate electromagnetic scattering from composite and complex bodies. This kind of solution combines 2 different techniques to explore the most efficient characteristics of the methods involved. The most common hybrid technique available in the literature combines FEM and MoM.[3,4] Although FEM is a method whose applicability, efficiency, and accuracy have been already reported in the literature, it requires the generation of a mesh. Despite the efforts that have been carried out to automate the process of mesh generation, a considerable computational effort is still

needed when the problem involves 3-dimensional complex geometries, especially those with media discontinuities or moving boundaries that cause severe deformations in elements, resulting in loss of precision.

Given those difficulties, a new class of differential equation methods, meshless methods (MM), which does not require a mesh structure, has been developed.[5] In these methods, the solution is obtained using only a cloud of nodes spread throughout the region of interest. This feature makes MM appropriate to deal with complex geometries and inhomogeneities. Among the MM available in the literature, the element-free Galerkin method (EFGM)[6] and meshless local Petrov-Galerkin method (MLPGM),[7,8] for example, have been extensively investigated, because they are extremely robust and have good convergence rates.

Therefore, the development of hybrid methods combining meshless methods, which do not require a mesh structure, and MoM, with unknowns to be determined only at the scatterer's surface, is an attractive way to deal with complex geometries and inhomogeneities in electromagnetic scattering problems. The IEFGM-MoM technique can accomplish this task using interpolating EFGM (IEFGM) and the electric field integral equation (EFIE).[9] The objective of the present work is to extend the hybrid technique of Resende et al[9] to include also the magnetic field integral equation (MFIE) and combinations between EFIE and MFIE, and further investigate the numerical efficiency of the several formulations in the simulation of electromagnetic scattering from dielectric cylinders. In Section 2, the geometry of the problem under investigation (TM plane wave scattering by a dielectric cylinder) is presented. In Sections 3 and 4, the numerical techniques used to simulate the fields inside (via IEFGM) and outside (via surface integral equations evaluated by MoM) the dielectric scatterer are discussed, respectively. The hybrid IEFGM-MoM technique, formulated by imposing the continuity of the tangential field at the scatterer surface, is detailed in Section 5. In Section 6, numerical results are presented for the hybrid technique with different surface integral equations and compared with analytical solutions to illustrate the usefulness and accuracy of the proposed technique. This work ends up with some brief conclusions in Section 7.

2 | 2D ELECTROMAGNETIC SCATTERING PROBLEM

The scattering by a z-directed infinitely long dielectric cylinder with relative electric permeability ε_r, relative magnetic permeability μ_r, and surrounded by free space, as illustrated in Figure 1, is the problem under analysis. Here, the cylinder has a circular cross section Ω, and Γ is its circular boundary, in which the unit normal vector is $\boldsymbol{n}$ and the tangential direction is $\boldsymbol{t}$. Because of the circular cross section, in this particular problem, $\boldsymbol{n}$ and $\boldsymbol{t}$ are the cylindrical directions ρ and ϕ, respectively. For a TM_Z normally incident plane wave, the total electric field E_z and equivalent electric surface current J_z have only the z component, while the equivalent magnetic surface current M_ϕ has only the ϕ component.[2]

The IEFGM-MoM technique divides the problem into interior and exterior regions. In the interior region, IEFGM is used to calculate the fields. In the exterior region, filled with a homogeneous medium (here assumed vacuum for simplicity), the field is calculated by EFIE, MFIE, or CFIE (ie, combination between EFIE and MFIE), which are solved by the MoM.[1] The fields are coupled across the interface of the scatterer by using appropriate boundary conditions. Therefore, as the region outside the scatterer is not considered in the computations, the size of the numerical domain is reduced. In the following sections, time variation is assumed $\exp(j\omega t)$, where ω is the angular frequency.

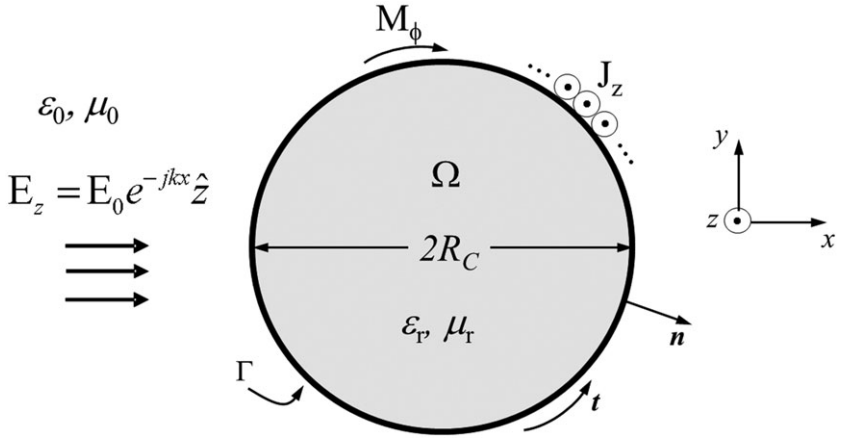

FIGURE 1 Cross section of infinitely long dielectric cylinder

3 | IEFGM FORMULATION—INTERNAL SUBPROBLEM

For the interior region of the scatterer, the IEFGM is used to solve the weak form of the 2D Helmholtz equation[10]:

$$\int_{\Omega}\left[(\nabla \mathrm{W}_E)\cdot\left(\mu_r^{-1}\nabla \mathrm{E}_z\right)-k_0^2\varepsilon_r \mathrm{W}_E \mathrm{E}_z\right]\, d\Omega-\int_{\Gamma}(\mathrm{W}_E \nabla \mathrm{E}_z\cdot\boldsymbol{n})\, d\Gamma = 0, \tag{1}$$

where k_0 is the wave number in vacuum and W_E is the IEFGM test function. Using Faraday's law, (1) can be modified to[3]:

$$\int_{\Omega}\left[(\nabla \mathrm{W}_E)\cdot\left(\mu_r^{-1}\nabla \mathrm{E}_z\right)-k_0^2\varepsilon_r \mathrm{W}_E \mathrm{E}_z\right]\, d\Omega- j\omega\mu_0\int_{\Gamma}\mathrm{W}_E\cdot \mathrm{J}_z\, d\Gamma = 0, \tag{2}$$

where E_z (in Ω) and J_z (in Γ) remain to be determined.

In the IEFGM, a shape function (SF) Φ is associated with a node placed over the domain of the problem, as illustrated in Figure 2 where the cylinder contour is represented by segments of size Δ. Each node I corresponds to a point located by $\mathbf{x}_I = (x_I, y_I)$, and each SF is zero over the whole domain, except near the corresponding node (ie, a SF has compact support). The unknown E_z and J_z can be approximated by their trial functions E_z^h and J_z^h[5]:

$$\mathrm{E}_z(\mathbf{x})\approx \mathrm{E}_z^h(\mathbf{x}) = \sum_{I=1}^{N}\Phi_I(\mathbf{x})\upsilon_I^E, \tag{3}$$

$$\mathrm{J}_z(\mathbf{x})\approx \mathrm{J}_z^h(\mathbf{x}) = \sum_{I=1}^{N_\Gamma}\Phi_I(\mathbf{x})\upsilon_I^J, \tag{4}$$

where $\mathbf{x} = (x, y)$, N is the number of SFs over $\Omega \cup \Gamma$, N_Γ is the number of SFs over Γ, and υ^E and υ^J are unknown coefficients. The discretized electric field $\mathrm{E}_z{}^h$ belongs to the finite-dimensional subspace V^N spanned by the SFs associated with all nodes in $\Omega\cup\Gamma$, whereas the discretized current $\mathrm{J}_z{}^h$ is sought in the finite-dimensional subspace spanned by the SFs associated with the nodes on the boundary Γ. The test function W_E is chosen according to the Galerkin method, ie, W_E also belongs to V^N and is expanded as:

$$\mathrm{W}_E(\mathbf{x})\approx \mathrm{W}_E^h(\mathbf{x}) = \sum_{U=1}^{N}\Phi_U(\mathbf{x})c_I, \tag{5}$$

where c_I are arbitrary constants.

Element-free Galerkin method couples the moving least squares (MLS)[11] approximation with the Galerkin weak form to obtain a domain-based MM. In the MLS, the local approximation function is defined as[5]:

$$\mathrm{X}_z^h(\mathbf{x}, \mathbf{x}_I) = \sum_{i=1}^{m} p_i(\mathbf{x}_I)a_i(\mathbf{x}) \equiv \mathbf{p}^T(\mathbf{x}_I)\mathbf{a}(\mathbf{x}), \tag{6}$$

where $\mathrm{X}_z{}^h$ is $\mathrm{E}_z{}^h$ or $\mathrm{J}_z{}^h$, m represents the number of monomial terms in the polynomial basis $\mathbf{p}^T(\mathbf{x}) = [1, x, y, \ldots]$, and $\mathbf{a}(\mathbf{x})$ are the unknown polynomial coefficients. In MLS approximation, the coefficients $\mathbf{a}(\mathbf{x})$ are determined by minimizing the following weighted discrete L^2 norm:

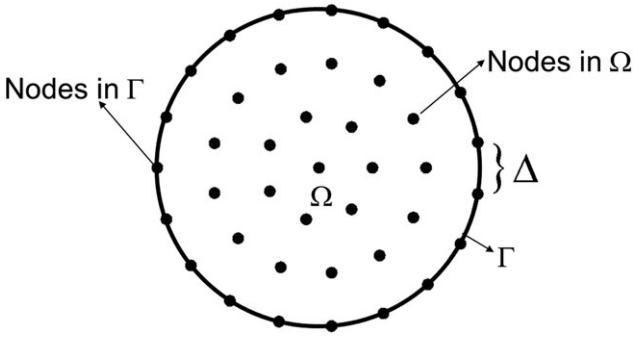

FIGURE 2 Node distribution in the computational domain

$$\mathfrak{I} = \sum_{I=1}^{NP} Q(r_I)\left[X_z^h(\mathbf{x},\mathbf{x}_I) - X_z(\mathbf{x}_I)\right]^2, \tag{7}$$

in which $Q(r_I)$ is the weight function, centered at the node $\mathbf{x}_I$, $r_I = |\mathbf{x} - \mathbf{x}_I|/d_I$, where $d_I = \alpha d_c$ is the node $\mathbf{x}_I$ influence domain size, $\alpha = 1.5$ is a scaling factor for the influence domain,[5] d_c is the average nodal distance associated with the node I, and NP is the number of nodes involved in the local approximation. By minimizing (7), Φ_I can be determined.

Although the MLS generates a smooth approximation for the unknown functions, its main weakness is the lack of the Kronecker delta property.[12,13] An interpolating MLS approximation (IMLS) can be obtained using singular weight functions in the definition of $\mathfrak{I}$ in (7). Thus, it is possible to obtain shape functions which satisfy the Kronecker delta property. Element-free Galerkin method using IMLS is called IEFGM. In this work, the following singular weight function is used[10]:

$$Q(r) = 1/(r^n + \beta^n), \tag{8}$$

where n and β are adjustable constants and r is associated to the support radius of the circular influence domain at each node. The IMLS singular weight function slope rate is adjusted by constant n and β to ensure no division by zero. In this work, the values of β and n were set to 0.1 and 10, respectively, according to the results of the parametric analysis performed in Resende and Coppoli,[10] which shows that for $\beta \leq 0.3$ and $n \geq 10$, the IEFGM convergence is guaranteed. Using (8), the shape functions Φ_I on Γ become triangular functions, because $\Phi_I = 1$ over node I and $\Phi_I = 0$ over nodes $I - 1$ and $I + 1$.

If the functions $E_z{}^h$ and $J_z{}^h$ satisfy the boundary conditions on Γ, Galerkin method leads to $Z^E(N \times N)$ and $Z^J(N \times N_\Gamma)$ matrices for which the elements are:

$$Z_{UI}^E = \int_\Omega \left[(\nabla\Phi_U)\cdot\left(\mu_r^{-1}\nabla\Phi_I\right) - k_0^2\varepsilon_r\Phi_U\Phi_I\right] d\Omega, \tag{9}$$

$$Z_{UI}^J = -j\omega\mu_0\int_\Gamma \Phi_U\Phi_I\, d\Gamma = 0. \tag{10}$$

4 | MOM FORMULATION—EXTERNAL SUBPROBLEM

For the exterior region, the equivalence principle is applied to establish the 2-dimensional EFIE and MFIE[2]:

$$\int_\Gamma \overline{W}\cdot\left\{\int_{\Gamma'}\left[k_0\eta_0 J_z G - j\nabla\times\left(M_\varphi G\right)\right] d\Gamma' - M_\varphi - E^i\right\} d\Gamma = 0, \tag{11}$$

$$\int_\Gamma \overline{W}\cdot\left\{\int_{\Gamma'}\left[\frac{k_0}{\eta_0}M_\varphi G + \frac{\nabla\left(\nabla\cdot M_\varphi G\right)}{\omega\mu_0} + j\nabla\times(J_z G)\right] d\Gamma' + J_z - H^i\right\} d\Gamma = 0, \tag{12}$$

respectively, where the 2-dimensional free-space Green's function $G = H_0^{(2)}(k_0R)/4$, $H_0^{(2)}$ is the second kind of Hankel function of order 0, $R = |\mathbf{x}–\mathbf{x}'|$ is the distance between observation ($\mathbf{x}$) and source ($\mathbf{x}'$) points, η_0 is the vacuum intrinsic impedance, E^i and H^i are the electric and magnetic incident fields, respectively, and $\overline{W}$ is the MoM weight function. In the adopted MoM technique, J_z and M_ϕ are described in triangular basis functions (TBF) distributed along Γ. Each TBF is defined over 2 consecutive segments, as illustrated in Figure 3. Therefore, the unknown current J_z is given by (4) and M_ϕ by:

$$M_\varphi(\mathbf{x}) = \sum_{I=1}^{N_\Gamma} \Phi_I\, v_I^M, \tag{13}$$

where v^M are unknown coefficients to be determined and N_Γ is the number of triangular shape functions over Γ. In (11) and (12), $\overline{W}$ is defined using Galerkin method, ie, the weight functions are also triangular functions Φ_U, leading to matrices $Z^{EJ}(N_\Gamma \times N_\Gamma)$, $Z^{EM}(N_\Gamma \times N_\Gamma)$, $V^E(N_\Gamma \times 1)$, $Z^{HJ}(N_\Gamma \times N_\Gamma)$, $Z^{HM}(N_\Gamma \times N_\Gamma)$, and $V^H(N_\Gamma \times 1)$ with elements given by[1]:

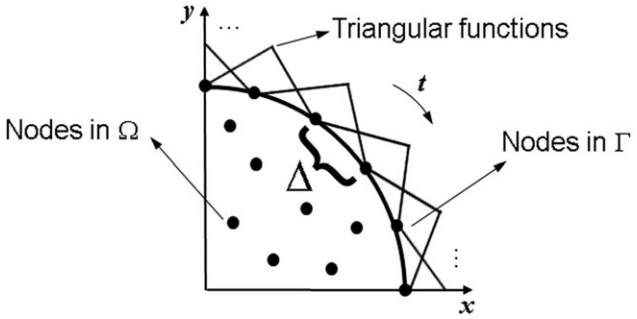

FIGURE 3 Triangular function distribution

$$Z_{UI}^{\mathrm{EJ}} = \frac{k_0\eta_0}{4}\int_{\Gamma}\int_{\Gamma'}\Phi_U\Phi_I H_0^{(2)}(k_0R)\,d\Gamma' d\Gamma, \tag{14}$$

$$Z_{UI}^{\mathrm{EM}} = \int_{\Gamma}\frac{\Phi_U}{2}d\Gamma\bigg|_{U=I} + \frac{jk_0}{4}\int_{\Gamma}\int_{\Gamma'}\Phi_U\Phi_I H_1^{(2)}(k_0R)\,\cos(\psi')\,d\Gamma' d\Gamma, \tag{15}$$

$$V_U^{\mathrm{E}} = \int_{\Gamma}\Phi_U E^i d\Gamma, \tag{16}$$

$$Z_{UI}^{\mathrm{HJ}} = \int_{\Gamma}\frac{\Phi_U}{2}d\Gamma\bigg|_{U=I} + \frac{jk_0}{4}\int_{\Gamma}\int_{\Gamma'}\Phi_U\Phi_I H_1^{(2)}(k_0R)\,\cos(\psi)\,d\Gamma' d\Gamma, \tag{17}$$

$$Z_{UI}^{\mathrm{HM}} = \frac{1}{4k_0\eta_0}\int_{\Gamma}\int_{\Gamma'}\left(k_0^2\Phi_U\Phi_I\, t\cdot t' + q\Delta^{-2}\right)H_0^{(2)}(k_0R)\,d\Gamma' d\Gamma, \tag{18}$$

$$V_U^{\mathrm{H}} = \int_{\Gamma}\Phi_U H^i d\Gamma, \tag{19}$$

in which $\psi(\psi')$is the angle between vectors $\boldsymbol{n}$ and $\mathbf{R}$ ($\boldsymbol{n}'$ and $\mathbf{R}$), $H_1^{(2)}$ is the second kind of Hankel function of order 1, and $q = 1$ or -1 if the segment has the Ith triangle side with positive or negative derivative, respectively. Equations (14) to (16) correspond to the EFIE (11) while (17) to (19) correspond to the MFIE (12). These sets of equations can be used individually, eg, (14) to (16) as in Resende et al,[9] or combined[3] to solve the equivalent external subproblem.

5 | IEFGM-MOM FORMULATION

The internal and external subproblems are coupled by enforcing the continuity of the total tangential electric (E_z) and magnetic (H_ϕ) fields at the scatterer's surface. The continuity of H_ϕ is imposed in the line integral of (2), where $J_z = \boldsymbol{n} \times H_\phi$. The continuity of E_z is imposed by[3]:

$$\int_{\Gamma}\overline{W}\cdot\left(E_z - \boldsymbol{n}\times M_\varphi\right)\,d\Gamma = 0, \tag{20}$$

where E_z and M_ϕ are described using triangular shape functions over Γ, such that E_z is still given by (3) replacing N by N_Γ, while M_ϕ is given by (13). Thus, (19) can be converted in $L^{\mathrm{E}}(N_\Gamma \times N)$ and $L^{\mathrm{M}}(N_\Gamma \times N_\Gamma)$ matrices with elements given by:

$$L_{UI}^{\mathrm{E}} = \int_{\Gamma}\Phi U\ \Phi I\ d\Gamma = -L_{UI}^{\mathrm{M}}. \tag{21}$$

Using (9), (10), (21), and combinations of (14) to (19), the following formulations are possible to find E_z, J_z, and M_ϕ: IEFGM-EFIE,[9] IEFGM-MFIE, IEFGM-CFIE, IEFGM-CFIE1, and IEFGM-CFIE2. Any of these formulations leads to a global sparse linear system of the form:

$$\begin{bmatrix} \mathrm{Z^E} & \mathrm{Z^J} & 0 \\ \mathrm{A} & \mathrm{B} & \mathrm{C} \\ 0 & \mathrm{E} & \mathrm{F} \end{bmatrix} \begin{bmatrix} \upsilon^E \\ \upsilon^J \\ \upsilon^M \end{bmatrix} = \begin{bmatrix} 0 \\ \mathrm{D} \\ \mathrm{G} \end{bmatrix}, \tag{22}$$

where A, B, C, D, E, F, and G for several formulations are presented in Table 1.

6 | NUMERICAL RESULTS

To evaluate the proposed techniques, dielectric circular cylinders with radii equal to $1\lambda_0$ and $2\lambda_0$ (λ_0 being the vacuum wavelength) and $\varepsilon_r = 2$ were chosen. The integrals in (14) to (19) were evaluated by 2-point (even number in Γ) and 3-point (odd number in Γ') Gaussian quadratures, to avoid singularity problems. In (10) and (20), the integrals were evaluated using only 1 point (middle point). For the integral in (9), an auxiliary rectangular cell structure was used in the calculations. To improve the coupling between internal and external subproblems, near the scatterer's surface, a larger number of Gauss integration points were adopted. Thus, as illustrated in Figure 4, in the ring R_e, 6×6 points per cell were used, while in the remaining region, 2×2 points per cell were used.

To investigate the accuracy of the numerical results with respect to analytical results, the average relative error $\mathrm{E_M}$ was adopted:

$$\mathrm{E_M}(X) = \frac{100}{N_P}\left|\frac{(X - AS)}{AS}\right| (\%), \tag{23}$$

$$\mathrm{ME_M} = \frac{\mathrm{E_M}(\mathrm{E_Z}) + \mathrm{E_M}(\mathrm{J_Z}) + \mathrm{E_M}(\mathrm{J_\varphi})}{3} (\%), \tag{24}$$

where X represents either $\mathrm{E_z}$, $\mathrm{J_z}$, or $\mathrm{M_\phi}$ numerical results, AS represents the analytical solution, and N_P is the number of points where the solution was obtained.

For the cylinder with radius equal to $1\lambda_0$, the values of $\mathrm{ME_M}$ obtained are presented in Figure 5 as a function of the number of nodes. As expected, for all investigated hybrid techniques, the $\mathrm{ME_M}$ values decrease as the number of nodes increase. The best result was found using IEFGM-CFIE formulation independent of the number of nodes used. The best performance of the IEFGM-CFIE is because, for the external subproblem, combinations between EFIE and MFIE avoid internal resonance problems. For the same cylinder, the IEFGM-MoM matrix condition number is shown in Figure 6. As one observes from Figure 6, for all hybrid techniques investigated in this work, the condition number does not increase significantly with the number of nodes and it is not significantly high for all formulations, which ensures the numerical stability of the several solutions. It is interesting to observe from Figure 6 that the best results were found for the IEFGM-CFIE, although for this formulation part of the main diagonal of (21) is equal to zero.

For the cylinder with radius $2\lambda_0$, the investigation was conducted with 20 398 nodes and 397 068 integration points. The values of $\mathrm{E_z}$, in a horizontal line Lx passing through the center of the cylinder along the x-axis, are presented in Figure 7A, while $\mathrm{J_z}$ and $\mathrm{M_\phi}$, over the cylinder's surface, are presented in Figure 7B, C, respectively. The results obtained

TABLE 1 Matrix elements of the IEFGM-MoM formulations

	EFIE	MFIE	CFIE	CFIE1	CFIE2
A	$\mathrm{L^E}$	$\mathrm{L^E}$	$\mathrm{L^E}$	$\mathrm{L^E}$	$\mathrm{L^E}$
B	0	0	0	$\mathrm{Z^{EJ}}$	$j\omega\mu_0\,\mathrm{Z^{HJ}}$
C	$\mathrm{L^M}$	$\mathrm{L^M}$	$\mathrm{L^M}$	$\mathrm{L^M} + \mathrm{Z^{EM}}$	$\mathrm{L^M} + j\omega\mu_0\,\mathrm{Z^{HM}}$
D	0	0	0	$\mathrm{V^E}$	$\mathrm{V^H}$
E	$\mathrm{Z^{EJ}}$	$\mathrm{Z^{HJ}}$	$\mathrm{Z^{EJ}} + \eta_0\mathrm{Z^{HJ}}$	$\mathrm{Z^{HJ}}$	$\mathrm{Z^{EJ}}$
F	$\mathrm{Z^{EM}}$	$\mathrm{Z^{HM}}$	$\mathrm{Z^{EM}} + \eta_0\mathrm{Z^{HM}}$	$\mathrm{Z^{HM}}$	$\mathrm{Z^{EM}}$
G	$\mathrm{V^E}$	$\mathrm{V^H}$	$\mathrm{V^E} + \eta_0\mathrm{V^H}$	$\mathrm{V^H}$	$\mathrm{V^E}$

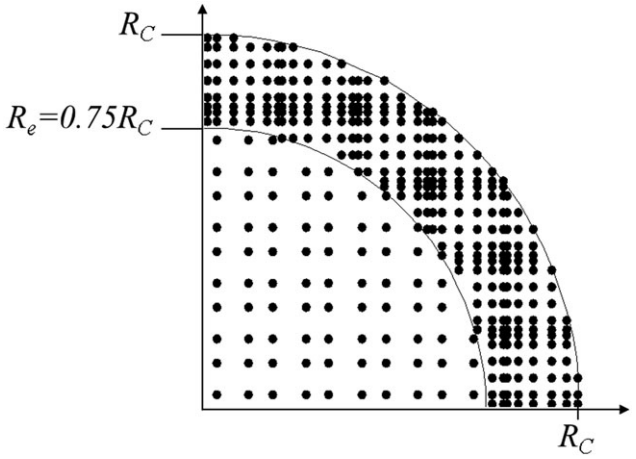

FIGURE 4 Integration point distribution

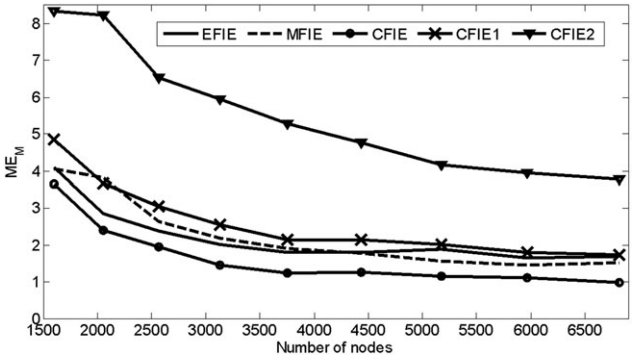

FIGURE 5 ME_M error for cylinder with radius equal to $1\lambda_0$

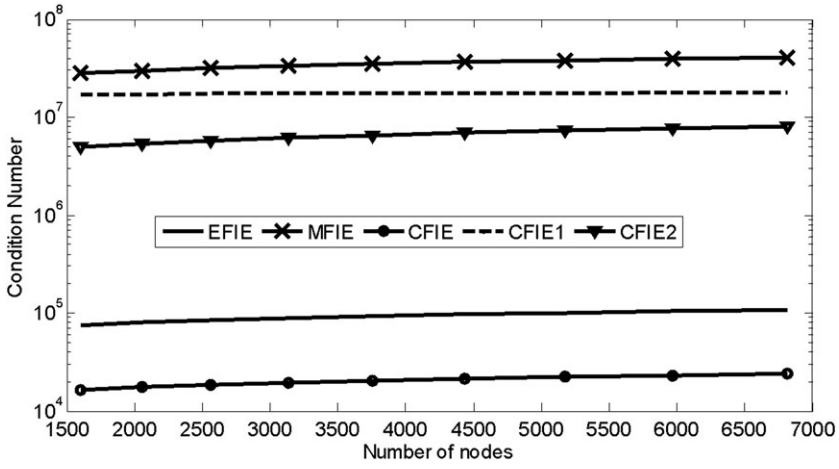

FIGURE 6 Condition number for cylinder with radius equal to $1\lambda_0$

from all formulations show good agreement with analytical solutions and demonstrate the accuracy of the proposed hybrid techniques. The values of E_M and ME_M are in Table 2, and the lowest value, $ME_M = 2.22\%$, was again obtained for IEFGM-CFIE, which is capable of eliminating internal resonance problems. For comparison purposes, using IEFGM-CFIE and 18 232 nodes, a cylinder with a higher $?_r = 10$ and radius equal to $1\lambda_0$ was considered and the numerical errors encountered were $E_M(E_z) = 2.67\%$, $E_M(J_z) = 2.17\%$, $E_M(M_\phi) = 2.29\%$, and $ME_M(E_z) = 2.24\%$, which show that the proposed technique is capable of handling moderately large dielectric constants. According to the results obtained from several simulations, numerical convergence is generally achieved when node densities greater than $600/\lambda^2$ (where λ is the wavelength inside the dielectric cylinder) are used.

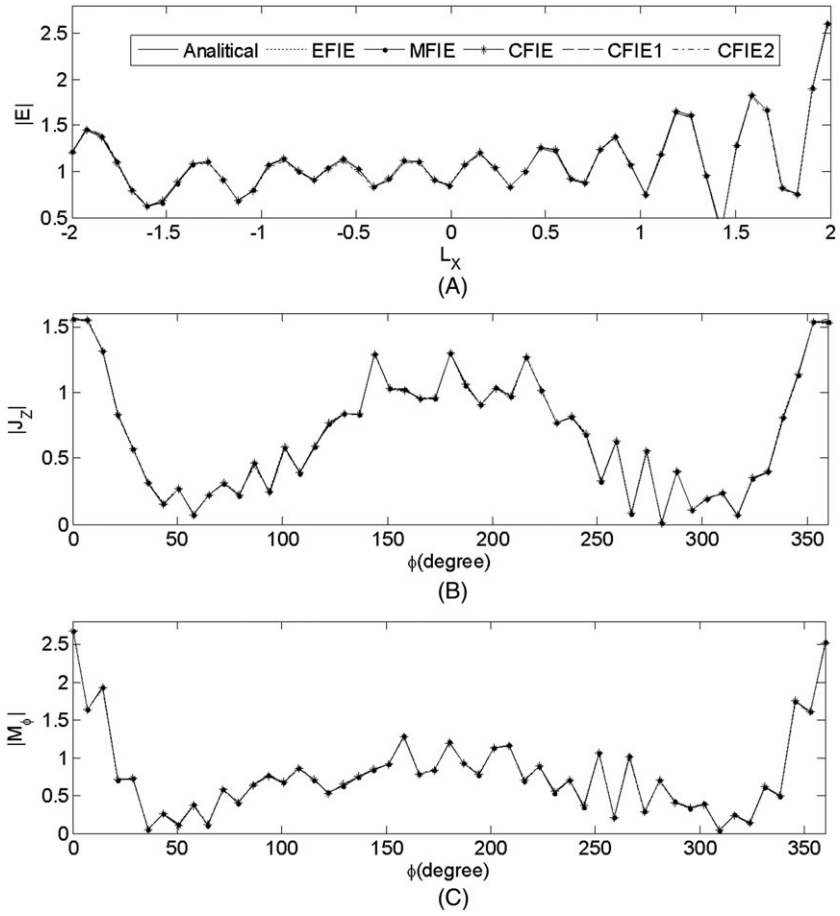

FIGURE 7 E_z, J_z, and M_f for cylinder with radius equal $2\lambda_0$

TABLE 2 E_M (%) and ME_M (%) for a cylinder with radius equal to $2\lambda_0$

		EFIE	MFIE	CFIE	CFIE1	CFIE2
	E_z	1.47	1.55	1.39	1.31	1.87
E_M	J_z	3.39	2.34	2.27	2.32	1.73
	M_ϕ	3.03	2.82	2.99	3.75	3.53
ME_M		2,63	2,24	2,22	2,46	2,38

7 | CONCLUSIONS

This work presented new formulations for hybrid technique IEFGM-MoM for solving 2D electromagnetic scattering. The validity and the accuracy of the formulations were confirmed by comparing numerical results against analytical solutions. When the resonance effects are expressive, all formulations lead to comparable accuracies. For cases where the internal resonant effects are relevant, IEFGM-CFIE is capable of eliminating such numerical resonances and leads to the most accurate results when compared with the other hybrid formulations. The proposed hybrid technique can be directly applied to the analysis of infinitely long dielectric cylinders with arbitrary cross-sectional shapes and may be extended to tridimensional problems with the appropriate change of Green's function.

ACKNOWLEDGEMENTS

This work was partially supported by the Brazilian agencies CNPq, FAPEMIG, and CAPES (PROCAD grant 068419/2014-01).

ORCID

Ursula do Carmo Resende http://orcid.org/0000-0003-0215-652X
Márcio Matias Afonso http://orcid.org/0000-0001-5462-7018

REFERENCES

1. Gibson WC. *The method of moments in electromagnetics*. 2nd ed. New York: CRC Press; 2015.
2. Peterson AF, Ray SL, Mittra R. *Computational methods for electromagnetics*. Piscataway: Wiley-IEEE Press; 1997.
3. Hoppe DJ, Epp LW, Lee JF. A hybrid symmetric FEM/MoM formulation applied to scattering by inhomogeneous bodies of revolution. *IEEE Trans Antennas Propag*. 1994;42(6):798-805. https://doi.org/10.1109/8.301698
4. Ilic MM, Djordjevic M, Ilic AZ, Notaros BM. Higher order hybrid FEM-MoM technique for analysis of antennas and scatterers. *IEEE Trans Antennas Propag*. 2009;57(5):1452-1460. https://doi.org/10.1109/TAP.2009.2016725
5. Liu GR. *Meshfree methods—moving beyond the finite element method*. Boca Raton: CRC Press; 2009.
6. Belytschko T, Lu YY, Gu L. Element-free Galerkin methods. *Int J Numer Methods Eng*. 1994;37(2):229-256. https://doi.org/10.1002/nme.1620370205
7. Nicomedes WL, Mesquita RC, Moreira FJS. A meshless local Petrov-Galerkin method for three-dimensional scalar problems. *IEEE Trans Magn*. 2011;47(5):1214-1217. https://doi.org/10.1109/TMAG.2010.2096203
8. Nicomedes WL, Mesquita RC, Moreira FJS. The meshless local Petrov-Galerkin method in two-dimensional electromagnetic wave analysis. *IEEE Trans Antennas Propag*. 2012;60(4):1957-1968. https://doi.org/10.1109/TAP.2012.2186223
9. Resende UC, Rosa CK, Avidago AG, Afonso MM, FJS Moreira. A new meshless-MoM hybrid method applied to the analysis of 2D electromagnetic scattering. 17th International Symposium on Electromagnetic Fields (ISEF 2015), Valencia, Spain.
10. Resende UC, Coppoli EHR, Afonso MM. A meshless approach using EFG interpolating moving least-squares method in 2-D electromagnetic scattering analysis. *IEEE Trans Magn* 2015, vol. 51, no. 3, 7200704. https://doi.org/10.1109/TMAG.2014.2361113., 1-4
11. Lancaster P, Salkauskas K. Surfaces generated by moving least squares methods. *Math Comput*. 1981;37(155):141-158. https://doi.org/10.2307/2007507
12. Marques GN, Machado JM, Verardi SLL, Stephan S, Preto AJ. Interpolating EFGM for computing continuous and discontinuous electromagnetic fields. *Compel*. 2012;26(6):1411-1438. https://doi.org/10.1108/03321640710823082
13. Coppoli EHR, Mesquita RC, Silva RS. Induction machines modeling with meshless methods. *IEEE Trans Magn*. 2012;48(2):847-850. https://doi.org/10.1109/TMAG.2011.2174211

How to cite this article: Resende UC, Moreira FJS, Afonso MM, Coppoli EHR. New formulations for the hybrid meshless-MoM method applied to 2D scattering problems. *Int J Numer Model*. 2019;32:e2479. https://doi.org/10.1002/jnm.2479